Journal of Biomedical Optics

BiomedicalOptics.SPIEDigitalLibrary.org

In vivo photoacoustic flowmetry at depths of the diffusive regime based on saline injection

Yong Zhou
Joemini Poudel
Guo Li
Lihong V. Wang

SPIE.

In vivo photoacoustic flowmetry at depths of the diffusive regime based on saline injection

Yong Zhou, Joemini Poudel, Guo Li, and Lihong V. Wang*
Washington University in St. Louis, Department of Biomedical Engineering, Optical Imaging Laboratory, 1 Brookings Drive, Campus Box 1097, St. Louis, Missouri 63130, United States

Abstract. We propose a saline injection-based method to quantify blood flow velocity *in vivo* with acoustic-resolution photoacoustic tomography. By monitoring the saline–blood interface propagating in the blood vessel, the flow velocity can be resolved. We first demonstrated our method in phantom experiments, where a root mean square error of prediction of 0.29 mm/s was achieved. By injecting saline into a mouse tail vein covered with 1 mm chicken tissue, we showed that the flow velocity in the tail vein could be measured at depths, which is especially pertinent to monitoring blood flow velocity in patients undergoing intravenous infusion. [DOI: 10.1117/1.JBO.20.8.087001]

Keywords: saline injection; blood flow velocity; acoustic-resolution photoacoustic tomography; intravenous infusion.

Paper 150337R received May 18, 2015; accepted for publication Jul. 20, 2015; published online Aug. 12, 2015.

Photoacoustic tomography (PAT) is a modality that provides imaging in either two dimensions (2-D) or three dimensions.[1–5] Combining the advantages of optical excitation and acoustic detection, PAT can image rich optical absorption contrast in biological tissues at depths. To date, PAT has been widely used for both structural and functional biological imaging in many different fields, including hematology,[6] oncology,[7] dermatology,[8] ophthalmology,[9] and gastroenterology.[10] Depending on the limiting factor for spatial resolution, PAT can be divided into optical-resolution PAT (OR-PAT) and acoustic-resolution PAT (AR-PAT). In OR-PAT, the optical focus is much tighter than the acoustic focus, and a high spatial resolution can be achieved. AR-PAT provides a lower spatial resolution, defined by the acoustic focus. Whereas in biological tissue ultrasound suffers much less scattering than light, AR-PAT can achieve deep imaging with a depth-to-resolution ratio of >100.[1] So far, with high resolution, OR-PAT has imaged a variety of important biological parameters *in vivo*, such as the oxygen saturation of hemoglobin (sO_2),[11] blood flow velocity,[12,13] pulse wave velocity,[14] and the metabolic rate of oxygen (MRO_2).[9] However, although AR-PAT has imaged sO_2 at depths, it still cannot provide *in vivo* blood flow information. In addition, in order to calculate MRO_2 with PAT, flow must be measured, which makes it even more important to quantify flow.

There are two fundamental reasons why it is difficult for AR-PAT to measure blood flow velocity. First, unlike ultrasound, PAT almost has no speckles.[15,16] If the target has a smooth boundary with respect to the wavelengths of the PA waves, the boundary signals of the target will stand out, while the speckles inside the target are largely suppressed. Because blood vessels in biological tissues usually have smooth boundaries, it is challenging for PAT to extract blood flow information merely based on speckle fluctuations. Second, AR-PAT has a lower spatial resolution than OR-PAT and, therefore, a larger detection voxel size. In typical OR-PAT, the spatial resolution is comparable to the size of red blood cells (RBCs). Thus, when RBCs flow into and out of the detection voxel, the PA signal changes are observable. By monitoring how fast the signal changes,[17] the flow velocity can be calculated. However, in AR-PAT, the large detection voxel contains many more RBCs than in OR-PAT. Because the number of RBCs inside the detection voxel can be assumed to follow a Poisson distribution,[18] a larger mean number of RBCs leads to a smaller relative RBC number change and, therefore, a smaller PA signal change. For example, if there are 10,000 RBCs in the detection voxel, the PA signal change due to the RBC number change would be only $\sim$1%, so the system would need a signal-to-noise ratio of >100 to measure the flow velocity.

Although challenging, different methods have been proposed to achieve blood flow measurement with AR-PAT, including PA Doppler (PAD) flowmetry[19–21] and ultrasonically encoded PA flowgraphy (UE-PAF).[22] Based on the PAD effect, different PAD shifts have been observed from particles moving with different flow speeds, and the Doppler theory allows the flow speeds to be calculated. However, to observe the PAD shift, the moving particles have to be very sparse. Thus, this method cannot measure the flow velocity of whole blood. But by using ultrasound to encode the PA signals, UE-PAF can achieve whole blood flow imaging in deep tissue. In UE-PAF, modulated ultrasound is focused into the blood vessel to create a heating source. Because PA signals are proportional to temperature, the PA signals from the heated area will increase.[23] By monitoring the increased PA signals along the blood vessel, the flow speed in the blood vessel can be measured. However, this method's complexity has limited it to phantoms and, to date, no *in vivo* data have been reported.

In this paper, we present a new method to measure blood flow velocity deep in biological tissues. To increase the PA signal changes due to flowing RBCs, saline is injected into the blood stream. As a result, at the saline–blood interfaces (SBIs),

*Address all correspondence to: Lihong V. Wang, E-mail: lhwang@wustl.edu

1083-3668/2015/$25.00 © 2015 SPIE

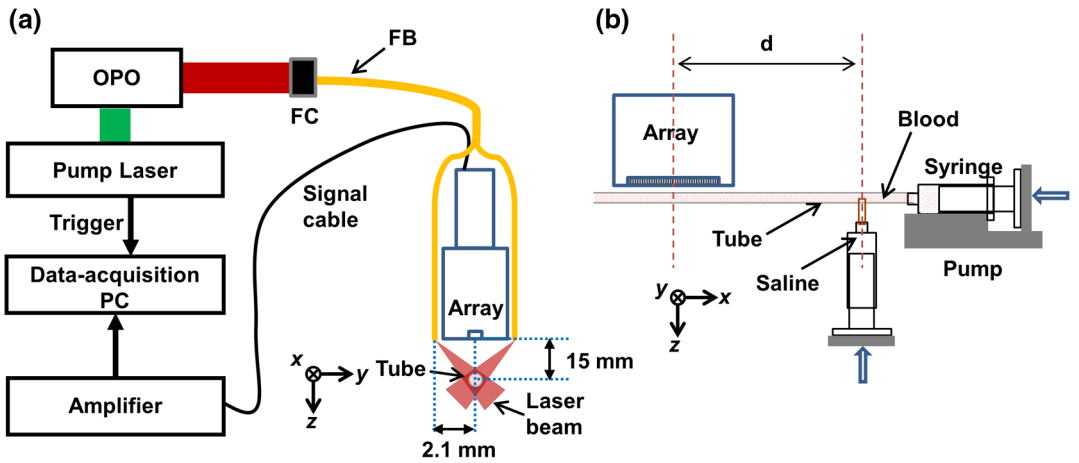

Fig. 1 Schematic of (a) the photoacoustic tomography system and (b) saline injection. FB, fiber bundle; FC, fiber coupler; OPO, optical parametric oscillator. *d* was 15 cm in the phantom experiment.

the PA signals have sharp changes—blood's PA signal is strong, while saline's signal is negligibly low. Thus, by monitoring the time course of the PA signals from the interface, the flow velocity in the blood stream can be quantified. In addition, because saline is widely used for intravenous infusion, no extra saline injection is needed in such patients.

We employed a typical AR-PAT system[24] to demonstrate this idea. As shown in Fig. 1(a), the light source was a tunable optical parametric oscillator laser with a repetition rate of 20 Hz. For deep tissue imaging, 680 nm light was chosen for the experiments. The light was first coupled into an optical fiber bundle, which was divided into two rectangular strips (20 mm × 1.25 mm) at the output end. The incident pulse fluence on the tissue surface was controlled to be ~10 mJ/cm^2, which was less than the safety limit set by the American National Standards Institute (20 mJ/cm^2) at this wavelength. A linear-array transducer containing 256 elements (LZ250, Visualsonics Inc.) was used to detect the PA signals. Thus, each laser pulse generated a two-dimensional (2-D) PA image. With a central frequency around 21 MHz and a 78% one-way bandwidth, this transducer array had an axial resolution of 86 μm. With a size of 23 mm × 3 mm and a cylindrical focus at 15 mm, this transducer array provided a lateral resolution of 119 μm and an elevational resolution of 1237 μm.[7]

Figure 1(b) shows a schematic of saline injection in phantom experiments. A silicone tube (300 μm inner diameter) filled with blood was used to mimic the blood vessel. The blood was pumped into the tube through a syringe, and the flow speed was controlled by a syringe pump. A second syringe was employed to perpendicularly inject saline solution into the tube. The distance between the injection point and the center of the field of view (FOV) was set to 15 cm, so the injection disturbance to the flow was minimized.

The flow velocity was extracted in three steps from the PA signals of the SBI. First, the whole process of the interface propagation through the FOV of the transducer array was monitored. At each time point, a 2-D image of the blood vessel was acquired and then converted to a one-dimensional (1-D) amplitude image via the Hilbert transformation, followed by taking the absolute value and then the peak amplitude. By piecing together all the 1-D images at consecutive time points, a final 2-D amplitude image of the SBI was achieved, as shown in Fig. 2(a). Note that the *x* axis is the displacement along the blood vessel and the *y* axis is time. Second, at each time point, the 1-D PA amplitude of the phantom blood vessel was fitted by an error function to extract the location of the SBI, as indicated by the mean value of the error function in Fig. 2(b). Last, by tracking the SBI along the phantom blood vessel, we calculated

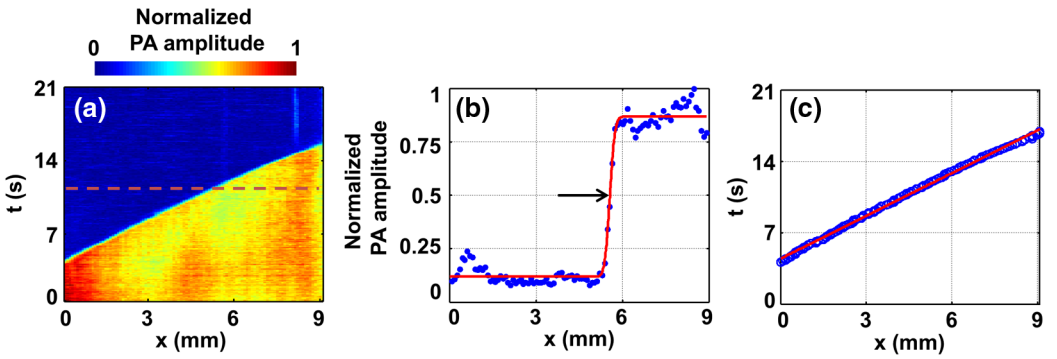

Fig. 2 Steps to extract the flow velocity. (a) Time course of the photoacoustic (PA) amplitude of the blood vessel in the phantom experiment. (b) Blue dots, one-dimensional PA amplitude along the dashed line in (a); red line, error function fitting; black arrow, the mean value of the error function. The mean value represents the saline–blood interface (SBI). (c) Blue circles, time course of the SBIs; red line, linear fitting.

the blood stream flow velocity. As shown in Fig. 2(c), although only two measurements of the SBI sufficed to calculate the blood flow velocity, multiple measurements could improve the accuracy by linear fitting.

Phantom experiments were first performed to demonstrate the capability of our method in flow measurement. To confirm that our method can measure blood flow in biological tissue at depths of the optical diffusive regime,[25] fresh chicken breast tissue with a thickness of ~2 mm was laid atop the phantom blood vessel. Figures 3(a)–3(c) show three representative 2-D amplitude images of the SBI, with blood stream flow velocities of 0.2, 1.3, and 4.5 mm/s. Because of the strong optical absorption difference between blood and saline, SBIs were imaged by PAT with high contrast, as shown in Figs. 3(a)–3(c). Thus, by linear fittings of the SBI spatial-temporal locations, our measured blood flow velocities agreed well with the preset values, as shown in Fig. 3(d). The root mean square error of prediction (RMSEP)[26] was calculated to be 0.29 mm/s, indicating that our method can measure deep blood flow with high accuracy. Thus, we concluded that our method should be able to measure blood flow velocity *in vivo*.

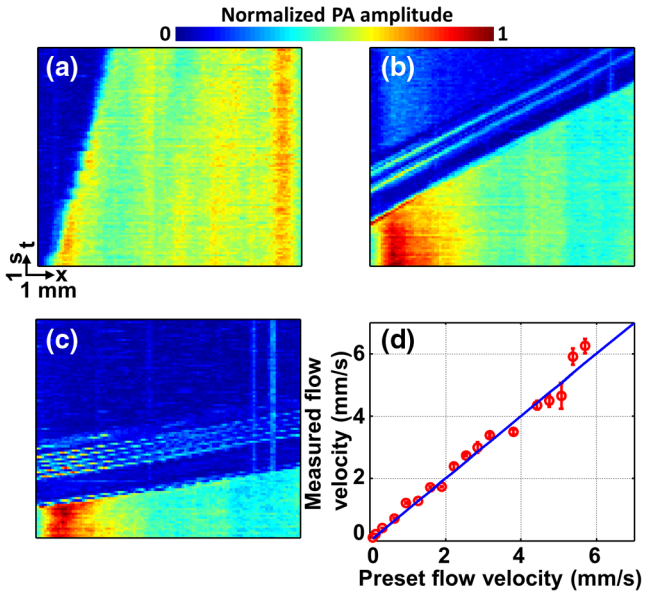

Fig. 3 Phantom experiments. Time course of the PA amplitude of the blood with flow velocity at (a) 0.2, (b) 1.3, and (c) 4.5 mm/s in a vessel. (d) Measured flow velocity versus preset flow velocity. Red circles, experimental measurement; blue line, ideal fit if the measured and preset velocities are identical.

We then measured blood flow velocity in a mouse tail vein *in vivo* to show the detection ability of the saline injection-based method. Again, a slice of chicken breast tissue (~1 mm) was put atop the tail vein to increase the measurement depth. Saline was injected into the tail vein with a home-made catheter to induce the SBI for blood flow measurement. The distance between the injection spot and the imaging window was ~3 cm. During the experiment, an infrared lamp kept the mouse warm, and a breathing anesthesia system (E–Z Anesthesia, Euthanex) kept the mouse motionless. All experimental animal procedures were carried out in conformity with laboratory animal protocols approved by the Animal Studies Committee of Washington University in St. Louis. As shown in Fig. 4(a), before saline injection, the whole tail vein in the FOV could be clearly observed. However, when the saline flushed in, there were almost no signals from the blood vessel because of the low absorption of saline, as shown in Fig. 4(b). The total SBI propagation process in the FOV is shown in Video 1. Again, the SBI's spatial-temporal location can be clearly imaged by PAT, as shown in Fig. 4(c). Based on the same procedure as in the phantom experiments, the blood flow velocity was quantified to be ~4.5 mm/s.

With an ~10 mm FOV along the lateral direction, the system has a frame rate of 10 Hz. Limited by the system's memory, a maximum of 1000 continuous frames can be stored. If we use the lateral resolution (119 μm) as the minimum displacement that the system can separate, the minimum flow speed the system can measure is ~119 μm/50 s = 2.38 μm/s. For the maximum flow speed, in theory it should be around 50 mm/s based on the current frame rate and FOV along the lateral direction. Here we require that the SBI be imaged twice in order to measure the flow speed, for both the minimum and maximum flow estimation.

In summary, to our knowledge and for the first time, we achieved deep blood flow measurement *in vivo* with AR-PAT. SBIs were created by injecting saline into the blood vessel, and the blood flow velocity was measured by monitoring a single SBI propagation in the blood stream. Our phantom experiments showed that we could achieve a highly accurate measurement of blood flow velocity in deep biological tissue, with an RMSEP of 0.29 mm/s. The *in vivo* mouse experiments indicated that we could potentially measure blood flow in

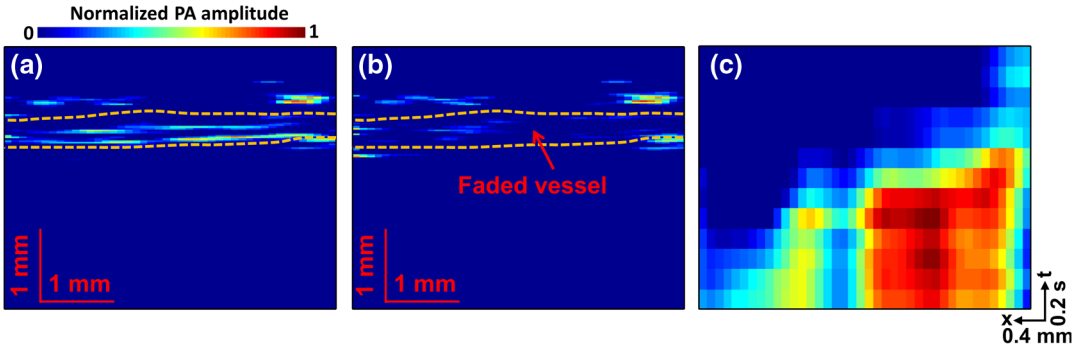

Fig. 4 *In vivo* experiments. PA images of the tail vein (a) before saline injection and (b) after saline injection. The saline propagation process is shown in (Video 1, MOV, 0.8 MB) [URL: http://dx.doi.org/10.1117/1.JBO.20.8.087001.1]. Dashed lines indicate the vessel region. (c) Time course of the PA amplitude of the tail vein when the saline flushed in.

humans. Based on saline injection, our method is particularly suitable for blood flow quantification in patients already undergoing intravenous infusion. Considering the difficulty that ultrasound encounters in measuring slow blood flow and sO_2, PA-based deep flow and sO_2 measurement opens a window for MRO_2 quantification in humans, which may lead to significant applications, such as noninvasive tumor screening and blood disorder diagnosis.

Acknowledgments

The authors would like to thank Professor James Ballard for manuscript editing. This work was sponsored in part by National Institutes of Health grants DP1 EB016986 (NIH Director's Pioneer Award), R01 CA186567 (NIH Director's Transformative Research Award), R01 EB016963, S10 RR026922, and R01 CA159959. L.V.W. has a financial interest in Microphotoacoustics, Inc. and Endra, Inc., which, however, did not support this work.

References

1. L. H. V. Wang and S. Hu, "Photoacoustic tomography: in vivo imaging from organelles to organs," *Science* **335**(6075), 1458–1462 (2012).
2. J. Xia and L. H. V. Wang, "Small-animal whole-body photoacoustic tomography: a review," *IEEE Trans. Biomed. Eng.* **61**(5), 1380–1389 (2014).
3. L. V. Wang, "Multiscale photoacoustic microscopy and computed tomography," *Nat. Photonics* **3**(9), 503–509 (2009).
4. P. Beard, "Biomedical photoacoustic imaging," *Interface Focus* **1**(4), 602–631 (2011).
5. V. Ntziachristos, "Going deeper than microscopy: the optical imaging frontier in biology," *Nat. Methods* **7**(8), 603–614 (2010).
6. M. Tang et al., "Noninvasive photoacoustic microscopy of methemoglobin in vivo," *J. Biomed. Opt.* **20**(3), 036007 (2015).
7. Y. Zhou et al., "Handheld photoacoustic probe to detect both melanoma depth and volume at high speed in vivo," *J. Biophotonics* **1**(7) (2015).
8. Y. Zhou et al., "Handheld photoacoustic microscopy to detect melanoma depth in vivo," *Opt. Lett.* **39**(16), 4731–4734 (2014).
9. W. Song et al., "A combined method to quantify the retinal metabolic rate of oxygen using photoacoustic ophthalmoscopy and optical coherence tomography," *Sci. Rep.* **4**(6525) (2014).
10. J. M. Yang et al., "Simultaneous functional photoacoustic and ultrasonic endoscopy of internal organs in vivo," *Nat. Med.* **18**(8), 1297 (2012).
11. B. Ning et al., "Simultaneous photoacoustic microscopy of microvascular anatomy, oxygen saturation, and blood flow," *Opt. Lett.* **40**(6), 910–913 (2015).
12. W. Song, W. Z. Liu, and H. F. Zhang, "Laser-scanning Doppler photoacoustic microscopy based on temporal correlation," *Appl. Phys. Lett.* **102**(20), 203501 (2013).
13. Y. Zhou et al., "Calibration-free in vivo transverse blood flowmetry based on cross correlation of slow time profiles from photoacoustic microscopy," *Opt. Lett.* **38**(19), 3882–3885 (2013).
14. C. H. Yeh et al., "Photoacoustic microscopy of blood pulse wave," *J. Biomed. Opt.* **17**(7), 070504 (2012).
15. Z. J. Guo, L. Li, and L. H. V. Wang, "On the speckle-free nature of photoacoustic tomography," *Med. Phys.* **36**(9), 4084–4088 (2009).
16. Z. J. Guo, Z. Xu, and L. H. V. Wang, "Dependence of photoacoustic speckles on boundary roughness," *J. Biomed. Opt.* **17**(4), 046009 (2012).
17. J. J. Yao et al., "In vivo photoacoustic imaging of transverse blood flow by using Doppler broadening of bandwidth," *Opt. Lett.* **35**(9), 1419–1421 (2010).
18. Y. Zhou et al., "Calibration-free absolute quantification of particle concentration by statistical analyses of photoacoustic signals in vivo," *J. Biomed. Opt.* **19**(3), 37001 (2014).
19. S. L. Chen et al., "Photoacoustic correlation spectroscopy and its application to low-speed flow measurement," *Opt. Lett.* **35**(8), 1200–1202 (2010).
20. H. Fang, K. Maslov, and L. V. Wang, "Photoacoustic Doppler effect from flowing small light-absorbing particles," *Phys. Rev. Lett.* **99**(18), 184501 (2007).
21. J. Brunker and P. Beard, "Pulsed photoacoustic Doppler flowmetry using time-domain cross-correlation: accuracy, resolution and scalability," *J. Acoust. Soc. Am.* **132**(3), 1780–1791 (2012).
22. L. D. Wang et al., "Ultrasonically encoded photoacoustic flowgraphy in biological tissue," *Phys. Rev. Lett.* **111**(20), 204301 (2013).
23. A. Sheinfeld and A. Eyal, "Photoacoustic thermal diffusion flowmetry," *Biomed. Opt. Express* **3**(4), 800–813 (2012).
24. A. Needles et al., "Development and initial application of a fully integrated photoacoustic micro-ultrasound system," *IEEE Trans. Ultrason. Ferr. Freq. Control* **60**(5), 888–897 (2013).
25. L. V. Wang and H. Wu, *Biomedical Optics: Principles and Imaging*, Wiley, Hoboken, New Jersey (2007).
26. Y. Zhou et al., "Photoacoustic microscopy of bilirubin in tissue phantoms," *J. Biomed. Opt.* **17**(12), 126019 (2012).

Yong Zhou is currently a graduate student in biomedical engineering at Washington University in St. Louis, under the supervision of Dr. Lihong V. Wang, Gene K. Beare Distinguished Professor. His research focuses on the development of photoacoustic imaging systems.

Joemini Poudel received his BASc in biomedical engineering from Simon Fraser University in Vancouver, Canada. He is currently a PhD student in biomedical engineering at Washington University in St. Louis. His research interest involves application of reconstruction algorithms for photoacoustic computed tomography and ultrasound computed tomography.

Guo Li is currently a postdoc at Washington University in St. Louis in Dr. Lihong V. Wang's lab. His research interests are in high-frequency linear-array photoacoustic imaging.

Lihong V. Wang is a Gene K. Beare Distinguished Professor at Washington University, has published 425 journal articles (h-index = 96, citations > 36,000), and delivered 420 keynote/plenary/invited talks. His laboratory published the first functional photoacoustic CT and three-dimensional photoacoustic microscopy. He received the Goodman Award for his *Biomedical Optics* textbook, NIH Director's Pioneer Award, OSA Mees Medal, IEEE Technical Achievement and Biomedical Engineering Awards, SPIE Britton Chance Biomedical Optics Award, and an honorary doctorate from Lund University, Sweden.